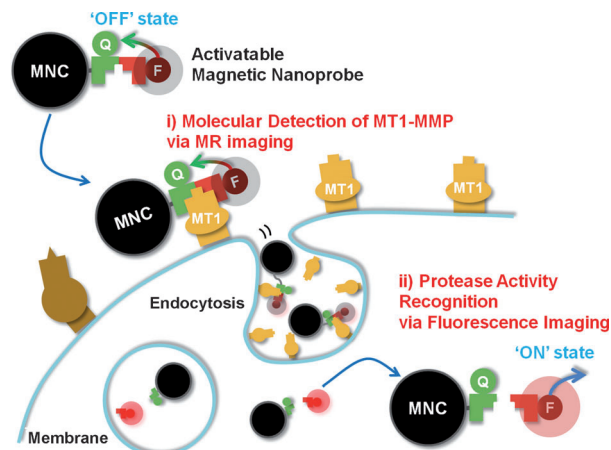


# Anchored Proteinase-Targetable Optomagnetic Nanoprobes for Molecular Imaging of Invasive Cancer Cells\*\*

Joseph Park, Jaemoon Yang, Eun-Kyung Lim, Eunjung Kim, Jihye Choi, Joo Kyung Ryu, Nam Hee Kim, Jin-Suck Suh, Jong In Yook, Yong-Min Huh,\* and Seungjoo Haam\*

Matrix metalloproteinases (MMPs) are attractive targets for molecular imaging because degrading and modifying the extracellular matrix by enzymatic activity is required for the invasive process of cancer cells.<sup>[1]</sup> Among the large family of MMPs, increasing evidence suggests that a subclass of the membrane-anchored proteinases, the membrane-type (MT) MMPs, plays dominant roles in controlling invasive cancer cell behavior.<sup>[2]</sup> In particular, MT1-MMP not only plays a direct and essential role in allowing tumor cells to invade into connective tissue,<sup>[2,3]</sup> but also provides a direct cellular target for molecular imaging to detect invasive cancer cells, in comparison with secreted, soluble MMPs.<sup>[1a,2,3]</sup>

Herein, we describe the development of a bimodal imaging probe enabling precise recognition of the expression of MT1-MMP anchored on invasive cancer cells and its protease activity simultaneously. MT1-MMP may be a targetable biomarker for a specific delivery and possesses proteolytic activity for certain substrates.<sup>[4]</sup> Activatable fluorogenic peptide (ActFP) was formulated as a targeting moiety and proteolytic ligand for MT1-MMP and conjugated with magnetic nanocrystals (MNCs), synthesized as magnetic resonance (MR) imaging contrast agents (Figure 1).<sup>[5]</sup> The magnetic and fluorogenic properties, based on the fluores-



**Figure 1.** The dual imaging process of activatable magnetic nanoprobes (magnetic nanocrystals conjugated with activatable fluorogenic peptides, MNC-ActFP) for i) molecular detection of MT1-MMP anchored on invasive cancer cells by MR imaging, and ii) sensitive recognition of the proteolytic activity of MT1-MMP by fluorescence imaging. Q = quencher, F = fluorescence dye.

cence resonance energy transfer (FRET) effect, of MNC-ActFP and their targeting potential were investigated to assess its capability as a multimode imaging probe.<sup>[6]</sup>

For targeted imaging of MT1-MMP anchored on invasive cancer cells and the measurement of the proteolytic activity, ActFP (Cy5.5-GPLPLRSWGLK(BHQ-3)) was designed and synthesized as both a MT1-MMP-specific substrate and a fluorescence imaging probe, based on the FRET effect (Supporting Information, Figure S1). First, a shorter fluorogenic peptide was prepared by labeling at both ends to form Cy5.5-GPLPLRSW(BHQ-3) amide. However, because of the bulky structures of Cy5.5 and BHQ-3, peptide cleavage was not observed. Considering this steric hinderance, we modified the fluorogenic peptide by inserting three amino acid sequence spacers (GLK) for effective cleaving to MT1-MMP (Supporting Information, Figure S2).<sup>[4a,7]</sup> MNCs, as MR imaging contrast agents, were synthesized by a thermal decomposition method and were coated with aminated polysorbate for the solubilization into the aqueous phase and the conjugation of ActFP.<sup>[8]</sup> After the conjugation of ActFP to the aminated MNCs using the carbodiimide EDC, the colloidal size of MNC-ActFP was  $42.3 \pm 1.2$  nm, by laser scattering, which was slightly larger than bare water-soluble MNCs ( $37.3 \pm 2.2$  nm). Furthermore, MNC-ActFP exhibited a negative surface charge at  $-8.2 \pm 3.7$  mV, which was converted from the positive surface charge of the aminated MNC ( $24 \pm 5.2$  mV) owing to the conjugation of anionic

[\*] J. Park,<sup>[†]</sup> E.-K. Lim, E. Kim, J. Choi, Prof. S. Haam  
Department of Chemical and Biomolecular Engineering  
Yonsei University, Seoul 120-749 (Republic of Korea)  
E-mail: haam@yonsei.ac.kr

Prof. J. Yang,<sup>[†]</sup> Prof. J.-S. Suh, Prof. Y.-M. Huh  
Department of Radiology, Yonsei University  
Seoul 120-752 (Republic of Korea)  
E-mail: ymhuh@yuhs.ac

J. K. Ryu, N. H. Kim, Prof. J. I. Yook  
Department of Oral pathology, Oral Cancer Research Institute  
Yonsei University, Seoul 120-752 (Republic of Korea)

Prof. J. Yang,<sup>[†]</sup> Prof. J.-S. Suh, Prof. Y.-M. Huh, Prof. S. Haam  
YUHS-KRIBB Medical Convergence Research Institute  
Seoul 120-752 (Republic of Korea)

Prof. J.-S. Suh, Prof. Y.-M. Huh  
Severance Biomedical Science Institute (SBSI)  
Seoul 120-749 (Republic of Korea)

[†] These authors contributed equally to this work.

[\*\*] This work was supported by the Korea Science and Engineering Foundation grant funded by the Korean government (M10755020001-07N5502-00110), the KRIBB Research Initiative Program (7-2009-0326), National Research Foundation of Korea Grant funded by the Korean Government (MEST) (2010-0019923) and a grant of the Korea Healthcare technology R&D Project, Ministry for Health & Welfare Affairs, Republic of Korea (A085136)  
Supporting information for this article is available on the WWW under <http://dx.doi.org/10.1002/anie.201106758>.

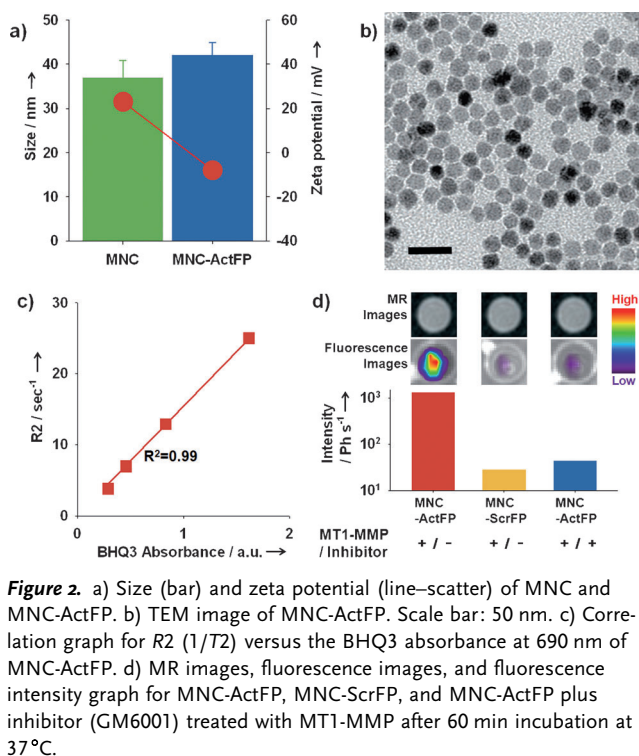


**Figure 2.** a) Size (bar) and zeta potential (line–scatter) of MNC and MNC-ActFP. b) TEM image of MNC-ActFP. Scale bar: 50 nm. c) Correlation graph for  $R2$  ( $1/T2$ ) versus the BHQ3 absorbance at 690 nm of MNC-ActFP. d) MR images, fluorescence images, and fluorescence intensity graph for MNC-ActFP, MNC-ScrFP, and MNC-ActFP plus inhibitor (GM6001) treated with MT1-MMP after 60 min incubation at 37 °C.

ActFP (Figure 2a). The morphology of MNC-ActFP was confirmed by a transmission electron microscopy (TEM) image (Figure 2b). The relaxivity coefficient ( $r2$ ) from the spin–spin relaxation time ( $T2$ ) weighted MR images for MNC-ActFP was  $404.75 \text{ mM}^{-1} \text{ s}^{-1}$  and MR signal sensitivity was linearly proportional to the concentration of BHQ3 from MNC-ActFP (Figure 2c).

To investigate the specificity and proteolytic activity of MT1-MMP, MNC-ActFP as a substrate was treated with MT1-MMP, MMP3, and MMP7 at 37 °C for 1 h. As seen in Figure 2d, MT1-MMP exhibited over 500-fold higher proteolytic activity for MNC-ActFP than other proteases (MMP3 and MMP7; Supporting Information, Figure S6). To assess the selectivity for MNC-ActFP, we also further prepared a scrambled fluorogenic peptide (ScrFP, Cy5.5-GPLPERSWGLK(BHQ-3)). MNC-ScrFP was formulated in a similar manner to MNC-ActFP. Figure 2d shows that MNC-ScrFP did not exhibit strong fluorescence intensity after treatment with MT1-MMP owing to the unrecognized peptide sequence. In the

presence of the broad-spectrum MMP inhibitor GM6001, the fluorescence intensity for MNC-ActFP was not increased, which is consistent with the fluorescence activity depending on the proteolytic activity of MT1-MMP. In MR images (Figure 2d), however, there was no signal difference for MNC-ActFP after treatment with each MMP. These results suggest that MNC-ActFP was suitable for the intended use with the combination of MNCs for MR imaging and the activatable fluorogenic probe. In particular, MNC-ActFP demonstrated specificity and sensitive proteolytic activity with MT1-MMP for the molecular imaging of invasive cancers.

We then determined the in vitro targeting potential and fluorogenic activity of MNC-ActFP for MT1-MMP-expressing cancer cells. First, the biocompatibility of MNC-ActFP was investigated using HT1080 cells expressing endogenous MT1-MMP. We found that MNC-ActFP was not toxic up to  $50 \mu\text{g mL}^{-1}$  (Supporting Information, Figure S7). MNC-ActFP was specifically attached to MT1-MMP-expressing HT1080 cells (Figure 3a); this was confirmed by  $T2$ -weighted MR imaging.  $\Delta R2/R2_{\text{nontreatment}}$  for HT1080 cells treated with MNC-ActFP was 263.1%, whereas MNC-ScrFP did not exhibit a significant increase in MR signal intensity ( $\Delta R2/R2_{\text{nontreatment}} = 18.4\%$ ; Figure 3b). Moreover, when the inhibitor (GM6001) was co-administered with MNC-ActFP to HT1080 cells, no increase in MR signal was observed, owing to the blocking of proteolysis of MT1-MMP by MNC-ActFP (Figure 3a,b). On the other hand, the magnetic ion (Fe + Mn) contents for HT1080 cells treated with MNC-ActFP, MNC-ScrFP, and MNC-ActFP plus inhibitor were measured by inductively coupled plasma atomic emission spectroscopy.

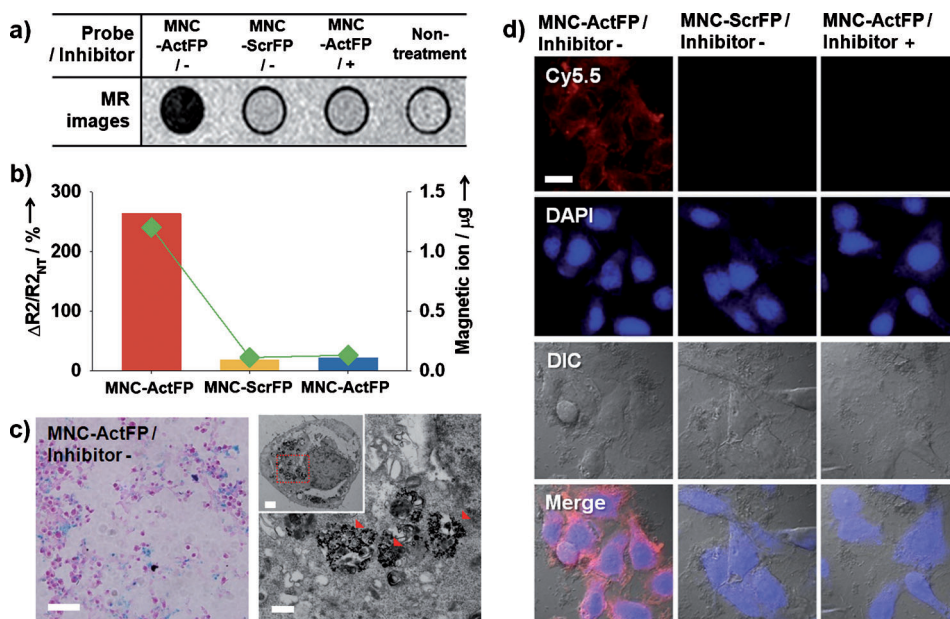


**Figure 3.** a)  $T2$ -weighted MR images for HT1080 cells treated with MNC-ActFP, MNC-ScrFP, and MNC-ActFP plus inhibitor (GM6001) and nontreated HT1080 cells. b)  $\Delta R2/R2_{\text{nontreatment}}$  (bar) and magnetic ion (Fe + Mn) quantification, based on ICP-AES analysis (line scatter) for HT1080 cells treated with MNC-ActFP, MNC-ScrFP, and MNC-ActFP plus inhibitor. c) Prussian blue stained image (left; scale bar: 100  $\mu\text{m}$ ) and TEM images (right; scale bar: 1  $\mu\text{m}$ ) for HT1080 cells treated with MNC-ActFP. Low-magnification TEM image (inset; scale bar: 10  $\mu\text{m}$ ). Much MNC-ActFP was seen in the cytoplasm (red arrows). d) Confocal microscopic images of HT1080 cells treated with MNC-ActFP, MNC-ScrFP, and MNC-ActFP plus inhibitor (scale bar: 1  $\mu\text{m}$ ). MT1-MMP (red, Cy5.5) and nucleus (blue, DAPI).

MNC-ActFP exhibited over sixfold larger binding efficiency versus the other conditions (MNC-ScrFP and MNC-ActFP plus inhibitor; Figure 3b, right axis). As expected, these results were consistent with the MR imaging data. Furthermore, Prussian blue stained images of HT1080 cells treated with MNC-ActFP showed the presence of a high iron content, compared with the other conditions (MNC-ScrFP and MNC-ActFP plus inhibitor; Figure 3c, left; Supporting Information, Figure S8). In particular, the cellular TEM image clearly showed that MNC-ActFP was predominantly localized in the cytoplasm (Figure 3c, right), which is most likely due to the uptake of MNC-ActFP by MT1-MMP-mediated endocytosis.

To evaluate the near infrared (NIR) fluorogenic potential of the prepared activatable probe (MNC-ActFP) induced by MT1-MMP, confocal microscopic images of HT1080 cells treated with probes (MNC-ActFP, MNC-ScrFP, and MNC-ActFP plus inhibitor, respectively) were obtained (Figure 3d). At 1 h after the incubation of HT1080 cells treated with MNC-ActFP, cellular NIR fluorescence from Cy5.5 was detected in the cytoplasm. In contrast, neither of the other conditions (MNC-ScrFP and MNC-ActFP plus inhibitor) showed any significant increase in NIR fluorescence signal intensity, even after 60 minutes of incubation, reflecting the high specificity and sensitivity of MNC-ActFP for MT1-MMP-expressing cells. To further confirm the specific proteolytic activity of MNC-ActFP for MT1-MMP, MCF-7 cells (a cell type that expresses minimal levels of endogenous MT1-MMP; Supporting Information, Figure S9) were transfected to express wild-type MT1-MMP. Thus, MNC-ActFP exhibited fluorogenic ability in MT1-MMP-expressing MCF-7 cells and a significant signal change was detected over a 60 min incubation. However, mock-transfected MCF-7 cells (vector only) and catalytic mutant MT1-MMP-transfected MCF-7 cells<sup>[9]</sup> did not exhibit NIR fluorescence, consistent with the fluorogenic activity depending on the catalytic activity of MT1-MMP. These results indicated that the MNC-ActFP had potential as a dual imaging probe (MR and NIR fluorescence imaging) specifically for MT1-MMP-expressing cancer cells.

To confirm the in vivo diagnostic utility of MNC-ActFP (recognition of protease expression and proteolytic activity), MR and NIR fluorescence imaging of molecular markers was explored using a MT1-MMP-expressing tumor-bearing mouse model. MR imaging for the tumor-bearing mice ( $1 \times 10^7$  HT1080 cells, the proximal thigh region) was performed at different time points (preinjection, 15 min, 1 h, 2 h, and 4 h) after the intravenous injection of MNC-ActFP (200  $\mu\text{g}$  Fe + Mn) into the tail vein. After the injection of MNC-ActFP, an immediate MR signal increase was evident and the signal gradually increased over 4 h. Moreover, MR signal-enhanced microvessels from the tumor were confirmed (red arrowheads in Figure 4a) and 49.7% of the  $\Delta R2/R2_{\text{preinjection}}$  value was confirmed at 4 h. In contrast, the control probes (MNC-ScrFP and MNC-ActFP plus inhibitor) showed no enhanced MR signal intensity at the tumor site (Supporting information, Figure S10).

For the multilateral recognition of MT1-MMP-expressing cancer cells, on the other hand, in vivo proteolytic activity based on MNC-ActFP was investigated by NIR fluorescence imaging. Similar to the in vivo MR imaging experiment,

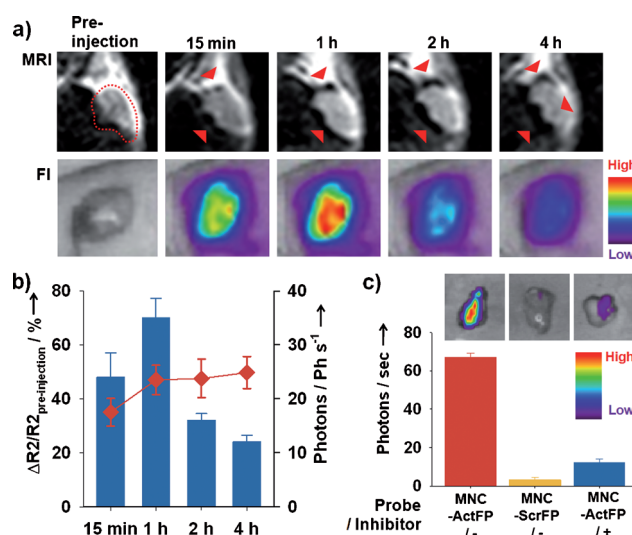


**Figure 4.** a) In vivo MR (upper) and NIR fluorescence (lower) images of tumor-bearing mice after intravenous injection of MNC-ActFP, MNC-ScrFP, and MNC-ActFP plus inhibitor (200  $\mu\text{g}$  Fe + Mn per mouse) at different time points (preinjection, 15 min, 1 h, 2 h, and 4 h). Red arrowheads in the MR images indicate the signal-enhanced sites of the tumor. b)  $\Delta R2/R2_{\text{non-treatment}}$  (line scatter) and NIR fluorescence intensity (bar graphs). c) NIR fluorescence images (upper) and their intensity graph (lower) for excised tumors from tumor-bearing mice 1 h after intravenous injection of MNC-ActFP, MNC-ScrFP, and MNC-ActFP plus inhibitor.

MNC-ActFP was injected intravenously into the tail vein of a MT1-MMP-expressing tumor-bearing mouse model. Sequential NIR fluorescence images ( $\lambda_{\text{emission}} = 690 \text{ nm}$ ) were obtained for 4 h after the injection of MNC-ActFP and a strong NIR fluorescence signal was seen in tumor sites (Figure 4a, lower panel). The maximum Cy5.5 signal in the tumor site was seen with 35 Phs<sup>-1</sup> at 1 h after the injection (Figure 4b). However, the control probes (MNC-ScrFP and MNC-ActFP plus inhibitor) showed no enhanced NIR fluorescence intensity (Supporting Information, Figure S11). Furthermore, depth profiles from the NIR fluorescence images were constructed by examining the intensity in slices cut along the  $z$  axis, which represented the two-dimensional slices, starting from  $z = 1$  to 7 mm depth. The fluorescence signal in tumor site was maximal between the depths of 3 and 5 mm (Supporting Information, Figure S12). Ex vivo NIR fluorescence imaging for extracted tumor tissue demonstrated that MNC-ActFP showed strong signal intensity in the tumor tissue compared with the other conditions (MNC-ScrFP and MNC-ActFP plus inhibitor; Figure 4c). Notably, the MR signal from MNC-ActFP was maintained for 4 h and the NIR fluorescence signal in tumor tissue was increased at 2 h after the injection of the fluorogenic probe. These results are consistent with the release of Cy5.5 from ActFP after the cleavage by MT1-MMP anchored on invasive cancer cells acting as a NIR fluorescence imaging probe and MNC taken up by cancer cells, by protease-mediated endocytosis, being detected by MR imaging.

In conclusion, we have developed a MT1-MMP-targetable fluorogenic magnetic nanoprobe (MNC-ActFP) for the simultaneous assessment of the expression and proteolytic

activity of MT1-MMP anchored on invasive cancer cells by MR and NIR fluorescence imaging. Trafficking of MT1-MMP as a target biomarker for the molecular imaging provides a matched imaging signal for the detection of invasive cancer cells and early metastatic cancer. Thus, a MT1-MMP-specific peptide sequence (GPLPLRSWGLK) was designed and synthesized to provide fluorogenic activity by the combination of a NIR dye and a quencher to induce a FRET effect. Thus, we believe that the developed nanohybrid, a combined fluorescence imaging probe and MR imaging contrast agent, may be used to increase the sensitivity and specificity of detecting invasive cancer cells in diagnostic and therapeutic interventions in human cancer patients.

Received: September 23, 2011

Published online: December 12, 2011

**Keywords:** cancer · fluorogenic probes · magnetic resonance imaging · MT1-MMP · nanoprobes

- [1] a) T. E. McCann, N. Kosaka, B. Turkbey, M. Mitsunaga, P. L. Choyke, H. Kobayashi, *NMR Biomed.* **2011**, *24*, 561; b) S. Lee, E.-J. Cha, K. Park, S.-Y. Lee, J.-K. Hong, I.-C. Sun, S. Y. Kim, K. Choi, I. C. Kwon, K. Kim, C.-H. Ahn, *Angew. Chem.* **2008**, *120*, 2846; *Angew. Chem. Int. Ed.* **2008**, *47*, 2804.
- [2] R. G. Rowe, S. J. Weiss, *Annu. Rev. Cell Dev. Biol.* **2009**, *25*, 567.
- [3] K. B. Hotary, E. D. Allen, P. C. Brooks, N. S. Datta, M. W. Long, S. J. Weiss, *Cell* **2003**, *114*, 33.
- [4] a) S. Ohkubo, K. Miyadera, Y. Sugimoto, K.-i. Matsuo, K. Wierzbica, Y. Yamada, *Biochem. Biophys. Res. Commun.* **1999**, *266*, 308; b) A. R. Clapp, I. L. Medintz, H. Mattoussi, *ChemPhys-Chem* **2006**, *7*, 47; c) A. Remacle, G. Murphy, C. Roghi, *J. Cell Sci.* **2003**, *116*, 3905.
- [5] I. L. Medintz, A. R. Clapp, F. M. Brunel, T. Tiefenbrunn, H. Tetsuo Uyeda, E. L. Chang, J. R. Deschamps, P. E. Dawson, H. Mattoussi, *Nat. Mater.* **2006**, *5*, 581.
- [6] a) J.-s. Choi, J. C. Park, H. Nah, S. Woo, J. Oh, K. M. Kim, G. J. Cheon, Y. Chang, J. Yoo, J. Cheon, *Angew. Chem.* **2008**, *120*, 6355; *Angew. Chem. Int. Ed.* **2008**, *47*, 6259; b) L. Frullano, C. Catana, T. Benner, A. D. Sherry, P. Caravan, *Angew. Chem.* **2010**, *122*, 2432; *Angew. Chem. Int. Ed.* **2010**, *49*, 2382; c) S. Mizukami, R. Takikawa, F. Sugihara, M. Shirakawa, K. Kikuchi, *Angew. Chem.* **2009**, *121*, 3695; *Angew. Chem. Int. Ed.* **2009**, *48*, 3641; d) J.-H. Park, G. von Maltzahn, E. Ruoslahti, S. N. Bhatia, M. J. Sailor, *Angew. Chem.* **2008**, *120*, 7394; *Angew. Chem. Int. Ed.* **2008**, *47*, 7284; e) T. D. Schladt, M. I. Shukoor, K. Schneider, M. N. Tahir, F. Natalio, I. Ament, J. Becker, F. D. Jochum, S. Weber, O. Köhler, P. Theato, L. M. Schreiber, C. Sönnichsen, H. C. Schröder, W. E. G. Müller, W. Tremel, *Angew. Chem.* **2010**, *122*, 4068; *Angew. Chem. Int. Ed.* **2010**, *49*, 3976; f) Y. Song, X. Xu, K. W. MacRenaris, X.-Q. Zhang, C. A. Mirkin, T. J. Meade, *Angew. Chem.* **2009**, *121*, 9307; *Angew. Chem. Int. Ed.* **2009**, *48*, 9143; g) M. K. Yu, Y. Y. Jeong, J. Park, S. Park, J. W. Kim, J. J. Min, K. Kim, S. Jon, *Angew. Chem.* **2008**, *120*, 5442; *Angew. Chem. Int. Ed.* **2008**, *47*, 5362; h) M. Nahrendorf, P. Waterman, G. Thurber, K. Groves, M. Rajopadhye, P. Panizzi, B. Marinelli, E. Aikawa, M. J. Pittet, F. K. Swirski, R. Weissleder, *Arterioscler. Thromb. Vasc. Biol.* **2009**, *29*, 1444.
- [7] S. Lee, K. Park, S.-Y. Lee, J. H. Ryu, J. W. Park, H. J. Ahn, I. C. Kwon, I.-C. Youn, K. Kim, K. Choi, *Bioconjugate Chem.* **2008**, *19*, 1743.
- [8] a) J. Yang, C.-H. Lee, H.-J. Ko, J.-S. Suh, H.-G. Yoon, K. Lee, Y.-M. Huh, S. Haam, *Angew. Chem.* **2007**, *119*, 8992; *Angew. Chem. Int. Ed.* **2007**, *46*, 8836; b) E.-K. Lim, J. Yang, J.-S. Suh, Y.-M. Huh, S. Haam, *J. Mater. Chem.* **2009**, *19*, 8958.
- [9] R. C. Domingues, M. P. Carneiro, F. C. R. Lopes, R. C. Domingues, L. M. B. da Fonseca, E. L. Gasparetto, *Am. J. Roentgenol.* **2009**, *192*, 1012.

Supporting Information

© Wiley-VCH 2012

69451 Weinheim, Germany

**Anchored Proteinase-Targetable Optomagnetic Nanoprobes for  
Molecular Imaging of Invasive Cancer Cells\*\***

*Joseph Park, Jaemoon Yang, Eun-Kyung Lim, Eunjung Kim, Jihye Choi, Joo Kyung Ryu,  
Nam Hee Kim, Jin-Suck Suh, Jong In Yook, Yong-Min Huh,\* and Seungjoo Haam\**

anie\_201106758\_sm\_miscellaneous\_information.pdf

## **Supporting Information**

### **S1. Preparation of an activatable fluorogenic peptide (ActFP)**

Based on the previously reported MT1-MMP substrate, GPLPLRSW<sup>[1]</sup>, we designed a MT1-MMP specific probe by combining the linker peptide and two fluorochromes, Cy5.5 and BHQ-3. First, a shorter fluorogenic peptide sequence was prepared by labeling of the N- and C-terminal ends with Cy5.5 and BHQ-3, respectively, to form Cy5.5-GPLPLRSW(BHQ-3) amide. Glycine and lysine were incorporated at both termini to provide chemical conjugation sites for the Cy5.5 dye and BHQ-3. However, the cleavaging did not allow for the bulky dye and quencher. Considering the bulky structures of Cy5.5 and BHQ-3, we found that a peptide containing at least a three-amino-acid sequence spacer was required for effective cleavaging to MT1-MMP (Figure S1). Thus, to achieve efficient quenching and affinity for MT1-MMP, we used a peptide substrate incorporating glycine-leucine-lysine spacer, forming Cy5.5-GPLPLRSWGLK(BHQ-3) as the fluorogenic probe for MT1-MMP (Figure S2).<sup>[2]</sup>

This peptide sequence was synthesized using standard solid-phase Fmoc peptide chemistry.<sup>[3]</sup> For site-specific conjugation of BHQ-3 to the primary amine of the lysine adjacent to the cleavable sequence after the selective conjugation of BHQ-3, succinimide ester in anhydrous dimethylformamide was added and reacted overnight, followed by extensive washing of the peptide resin. Subsequently, the last Fmoc group was removed from the peptide resin and Cy5.5 succinimide ester was coupled to the N-terminal glycine (Figure S2). After deprotecting and cleaving the peptide from the resin, using trifluoroacetic acid, the resulting product was characterized. Optical properties of Cy5.5 and ActFPs were confirmed at  $\lambda_{\text{ex}}$  of 675 nm using a fluorescence imaging tool (eXplore Optix, Advanced Research Technologies Inc., Montreal, Canada; Figure S3) and MT1-MMP-specific fluorogenic effects of ActFPs were confirmed using Optix (Figure S4).

### **S2. Preparation of aminated magnetic nanocrystals (MNCs)**

To fabricate the fluorogenic magnetic nanoprobe [magnetic nanocrystals conjugated with activatable fluorogenic peptides (ActFPs), MNC-ActFPs], aminated MNCs were prepared. 10 mg of MNCs ( $\text{MnFe}_2\text{O}_4$ ) synthesized by thermal decomposition,<sup>[4]</sup> were dissolved in 4 mL of chloroform. Then, the organic phase was added into a 20 mL aqueous solution containing 100 mg of tri-aminated polysorbate.<sup>[5]</sup> After mutual saturation of the organic and continuous phase, the mixture was emulsified for 15 min with an ultrasonicator (Sae Han SH-2100, Korea) at 190 W.<sup>[4]</sup> After evaporation of the organic solvent, aminated MNCs were purified using a centrprep (3,000 $\times$ g, 30 min, MWCO 10,000) and were dispersed in an aqueous phase and stored for later use. The colloidal size of aminated MNCs was measured by laser scattering (Otsuka Electronics ELS-8000, Osaka, Japan) and the colloidal stability of aminated MNCs was maintained for over 3 months. Moreover, the aminated MNCs exhibited a strong superparamagnetic behavior, confirmed using a vibration sample magnetometer (MODEL-7407, Lakeshore) (Figure S5). The unit of magnetization was described in  $\text{emu g}^{-1}$  (whole particle weight).

### **S3. Preparation of fluorogenic magnetic nanoprobe (MNC-ActFPs)**

The aminated MNCs were chemically conjugated with the activatable fluorogenic peptides (ActFPs). The aminated MNCs (400  $\mu\text{g}$  MnFe) were dispersed in 1 mL of phosphate buffered saline (PBS) buffer (pH 7.4).

Subsequently, 1-ethyl-3-(3-dimethylaminopropyl)-carbodiimide (1.2 mg) and sulfo-N-hydroxysulfosuccinimide (1.5 mg) dissolved in 100  $\mu$ L of PBS (pH 7.4) were added to the MNCs solution and the reaction mixture was agitated for 20 min at room temperature. ActFPs (2.1 mg) was then added to the reaction solution and the reaction was continued at room temperature in the dark room for 6 h. By-products and unreacted peptide molecules were removed using a centrprep (6,000 rpm, 30 min). An absorption titration of the fluorogenic peptide was conducted to assess the amount of peptide bound to the polymeric nanoparticle surface using a UV-vis spectrometer (Optizen 2120UV, Mecasys Co.). The absorption intensity of BHQ-3 (650 nm) was calibrated and the concentration of bound peptide substrate was determined from known concentrations using a standard curve.

#### **S4. Fluorogenic effect of MNC-ActFPs**

The fluorescence recovery of MNC-ActFPs was examined in terms of MT1-MMP enzyme specificity and concentration of MT1-MMP or other MMP enzymes. Each MMP enzyme (MMP-3, 7 or MT1-MMP) was activated by incubation at 37°C for 1 h with a buffer solution (150 mM NaCl, 50 mM Tris-HCl, 5 mM CaCl<sub>2</sub>, and 0.025 % Brij-35, pH 7.5). The same amount of MNC-ActFPs was added to MMP enzyme solution and incubated at 37°C for an additional 1 h. The intensity of the recovered fluorescent signal, which depended on the concentration of MMP enzyme or probe, was monitored using the Xplore Optix system (Advanced Research Technologies Inc.) in the wavelength range of 680-800 nm over time, with excitation at 675 nm.

#### **S5. Cell viability assay by MTT**

The biocompatibility of the prepared MNC, MNC-ActFPs for target cancer cells was quantified by a colorimetric assay based on the mitochondrial oxidation of 3-(4,5-dimethylthiazolyl-2)-2,5-diphenyltetrazolium bromide (MTT). In a typical experiment, HT1080 cells were harvested at a density 10<sup>4</sup> cells/200  $\mu$ L in a 96-well plate and incubated at 37°C in a 5% CO<sub>2</sub> atmosphere. The cells were incubated for 24 h with MNC-ActFPs, rinsed with 100  $\mu$ L PBS (pH 7.4, 1 mM), and then treated with freshly prepared MTT solution (10  $\mu$ L) and incubated for an additional 4 h before adding 100  $\mu$ L dimethyl sulfoxide. After 24 h, the plates were assayed using an enzyme-linked immunosorbent assay (Spectra Max 340, Molecular Devices, USA) and the results were measured at an absorbance wavelength of 575 nm and a reference wavelength of 650 nm (Figure S7).

#### **S6. In vitro targeting study**

The targeting efficiency of MNC-ActFPs was investigated by magnetic resonance (MR) and fluorescence imaging. HT1080 cells (high MT1-MMP expression) and various MCF7 cells (wild-type, catalytic mutant, mock-transfected) were cultured in Dulbecco's modified Eagle's medium (DMEM; Gibco, USA) supplemented with 10% fetal bovine serum (FBS) and 1% antibiotics in a 5% CO<sub>2</sub> atmosphere. Target cells (HT1080 and MCF7 cells, 5.0 $\times$ 10<sup>6</sup> cells) were collected and washed in triplicate using blocking buffer (0.2% FBS and 0.02% NaN<sub>3</sub> in phosphate-buffered solution, pH 7.4, and 10 mM) to avoid non-specific binding. Then, they were incubated and

treated with ActFP and ScrFPs at 4°C. For the inhibition test, 100  $\mu$ M of GM6001 (1 mg/mL, galardin or ilomastat; Calbiochem) was pre-treated to block MT1-MMP on the cell surface. After 30 min, the solution was washed away three times. MR and fluorescence imaging was performed after the cells were resuspended in 200  $\mu$ L of 4% paraformaldehyde.

### **S7. Animal model**

HT1080 cells were cultured in DMEM (Gibco) supplemented with 10% FBS(Gibco) and 1% penicillin/streptomycin (PS, Gibco) in a 5% CO<sub>2</sub> atmosphere. The suspension of HT1080 cells ( $1 \times 10^7$  cells) in 50  $\mu$ L PBS (pH 7.4, 1 mM) was injected subcutaneously into the proximal thigh of male BALB/c-nude mice. All experiments were conducted with the approval of the Association for Assessment and Accreditation of Laboratory Animal Care International.

### **S8. MR imaging.**

We performed MR imaging experiments with a 1.5-T clinical MRI instrument with a micro-47 surface coil (Intera; Philips Medical Systems, Best, the Netherlands). R2 relaxivities of MNC-ActFPs, MNC-ScrFPs, and MNC-ActFPs + inhibitors were measured using the Carr-Purcell-Meiboom-Gill sequence at room temperature: TR = 10 s, 32 echoes with 12 ms even echo space, number of acquisition = 1, point resolution of  $156 \times 156 \mu\text{m}$ , section thickness of 0.6 mm. R2 was defined as  $1/T_2$  with units of  $\text{s}^{-1}$ . For T2-weighted MR imaging of cells in vitro at 1.5 T, the following parameters were used: point resolution:  $156 \times 156 \mu\text{m}$ , section thickness of 0.6 mm, TE = 60 ms, TR = 4000 ms, number of acquisitions = 1. For T2 mapping of cells in vitro, the following parameters were used: point resolution of  $156 \times 156 \mu\text{m}$ , section thickness of 0.6 mm, TE = 20, 40, 60, 80, 100, 120, 140, 160 ms, TR = 4000 ms, number of acquisitions = 2. The concentration of magnetic component was obtained and calculated with Fe + Mn.

In vivo MR imaging experiments were also performed with a 3-T clinical MRI instrument with a micro-47 surface coil (Philips Medical Systems). The T2-weighted MR images of nude mice injected with the prepared materials at 3T were acquired using the following parameters at room temperature: TR = 4,000 ms even echo space, number of acquisitions = 1, point resolution of  $312 \times 312 \mu\text{m}$ , section thickness of 0.6 mm and TE = 60 ms. The results shown are the average  $\pm$  standard deviation.

### **S9. In vivo fluorescence imaging**

We performed in vivo fluorescence imaging and tomography using MNC-ActFPs, MNC-ScrFPs, and MNC-ActFPs + inhibitor. After the intravenous injection of each sample, the fluorescence recovery profiles in HT1080 tumor-bearing mice were imaged by positioning mice on an animal plate, heated to 37°C, in the eXplore Optix system. The animal was automatically moved to the imaging chamber for scanning. Laser power and count time settings were optimized at 30  $\mu$ W and 0.1 s per point, respectively. Excitation and emission spots were raster-scanned in 1 mm steps over the selected region of interest to generate emission wavelength scans. A 670-nm pulsed laser diode was used to excite the Cy5.5 molecules. NIR fluorescence emission data were collected at 700 nm and detected with a fast photomultiplier tube (Hamamatsu, Japan) and time-correlated single photon counting system.

(Becker and Hickl GmbH, Berlin, Germany). Tumor contrast was measured by dividing the fluorescence intensities at the tumor area (T) and normal tissue area (N). All data, including whole body and two-dimensional (2D) slice images, were calculated using the region of interest function of the Analysis Workstation software. To analyze the depth profiles from the fluorescence images, the three-dimensional (3D) images were constructed by examining the intensity in slices cut along the  $z$ -axis, which represented the 2D slices, starting from  $z = 1$  to 7 mm deep (Figure S6). For ex vivo NIR fluorescence imaging, tumor sections were viewed using the Xplore Optix system. The excitation wavelength was 650 nm.

## References

- [1] S. Ohkubo, K. Miyadera, Y. Sugimoto, K.-i. Matsuo, K. Wierzbka, Y. Yamada, *Biochemical and Biophysical Research Communications* **1999**, 266, 308.
- [2] S. Lee, K. Park, S.-Y. Lee, J. H. Ryu, J. W. Park, H. J. Ahn, I. C. Kwon, I.-C. Youn, K. Kim, K. Choi, *Bioconjug Chem.* **2008**, 19, 1743.
- [3] R. B. Merrifield, *J. Am. Chem. Soc.* **1963**, 85, 2149.
- [4] J. Yang, C.-H. Lee, H.-J. Ko, J.-S. Suh, H.-G. Yoon, K. Lee, Y.-M. Huh, S. Haam, *Angew. Chem.-Int. Edit.* **2007**, 46, 8836.
- [5] E.-K. Lim, J. Yang, J.-S. Suh, Y.-M. Huh, S. Haam, *J Mater Chem.* **2009**, 19, 8958.

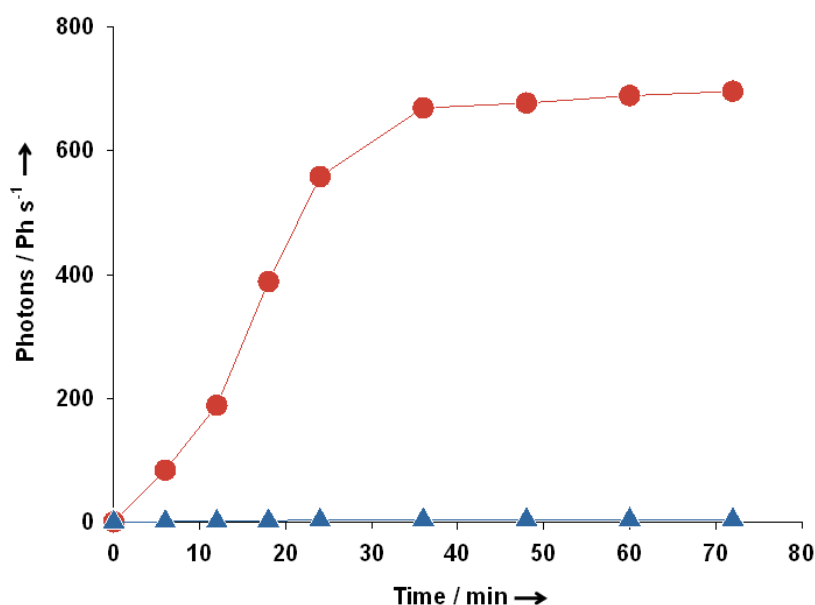


Figure S1. Fluorogenic efficiency induced by MT1-MMP for Cy5.5-GPLPLRSW(BHQ-3) (blue triangle) and Cy5.5-GPLPLRSWGLK(BHQ-3) (red circle).

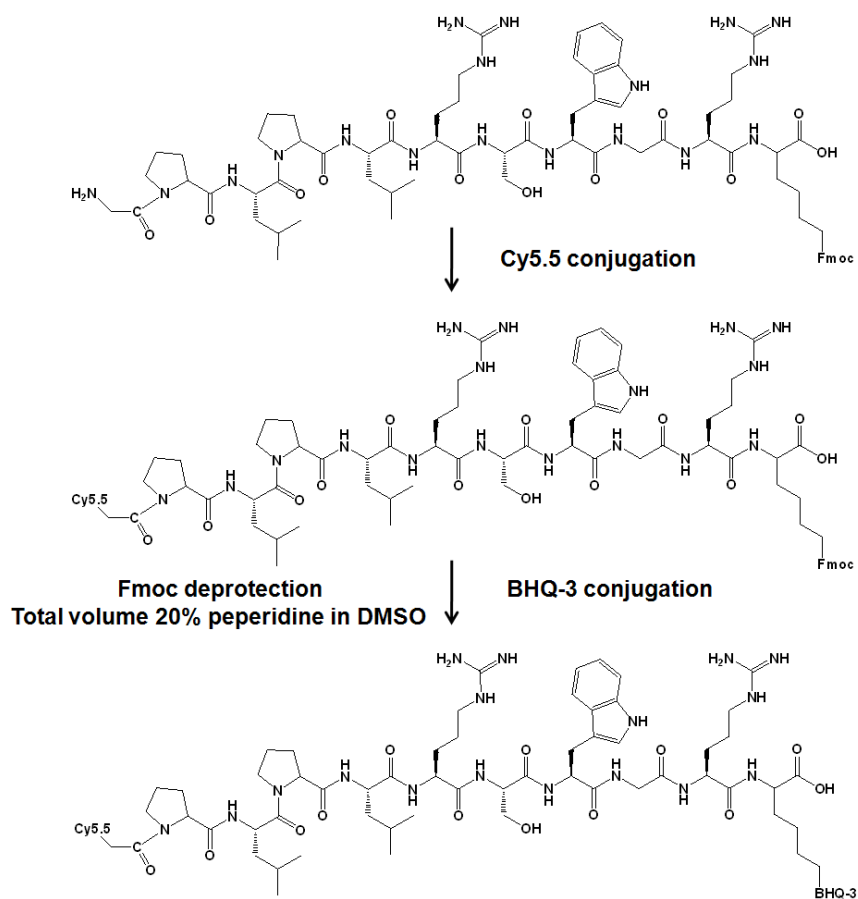


Figure S2. Synthetic scheme for ActFPs [Cy5.5-GPLPLRSWGLK(BHQ-3)].

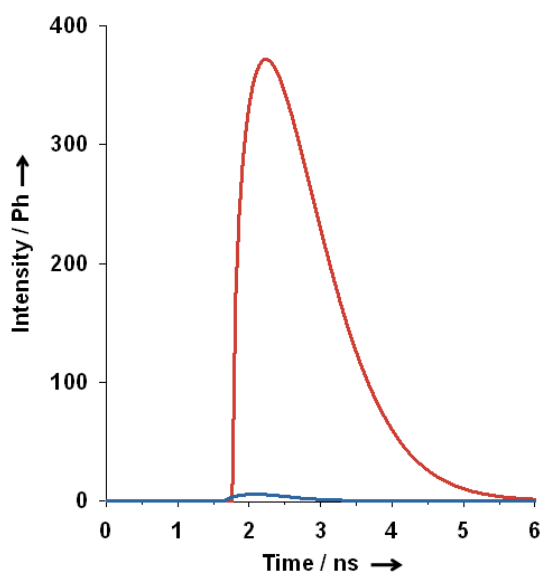


Figure S3. Fluorescence intensity for Cy5.5 (red line) and ActFPs (blue line).  $\lambda_{\text{ex}} = 675 \text{ nm}$ .

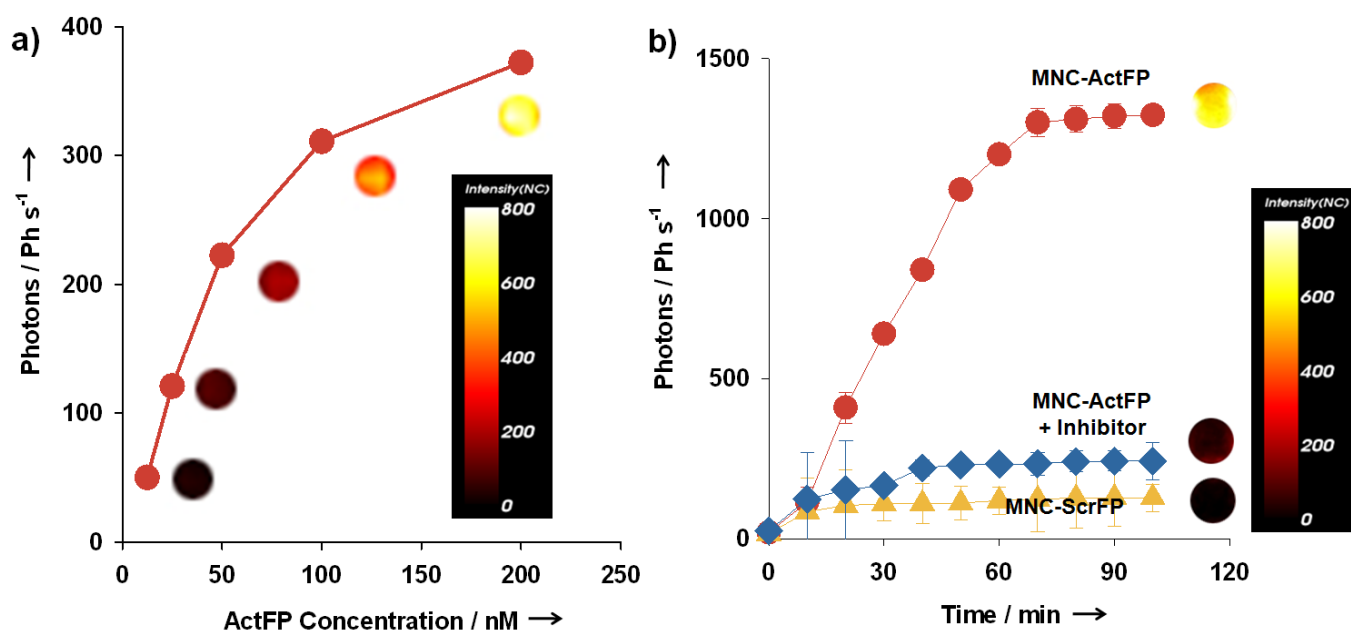


Figure S4. Fluorogenic effect for a) the different concentrations of ActFPs after the treatment of MT1-MMP and b) time-dependent fluorogenic effects for ActFP (red circle), ScrFP (yellow triangle), and ActFP with inhibitor (GM6001; blue square) treated with MT1-MMP.

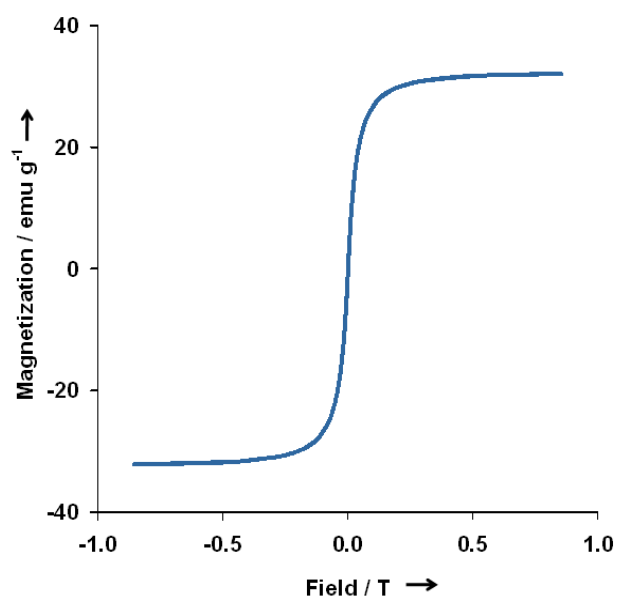


Figure S5. Magnetic hysteresis loops of MNC-ActFPs.

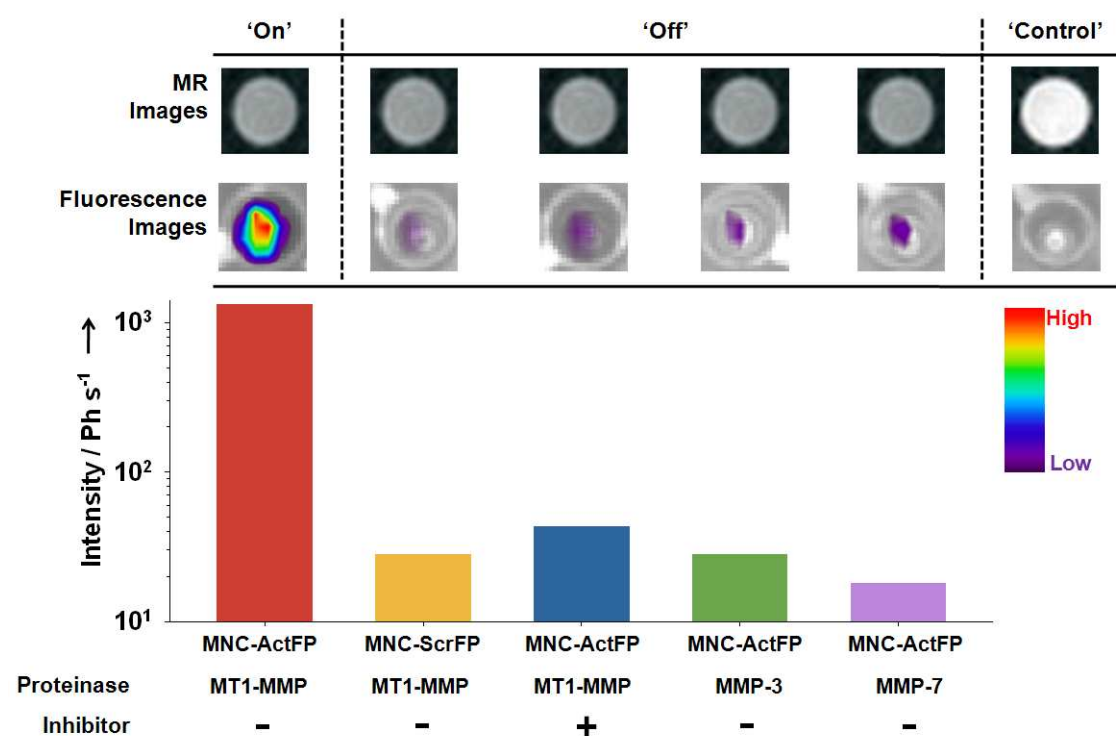


Figure S6. MR images, fluorescence images, and fluorescence intensity graph for MNC-ActFP, MNC-ScrFP, and MNC-ActFP with inhibitor (GM6001) treated with MT1-MMP, MMP-3, and MMP-7 after 60 min incubation at 37°C.

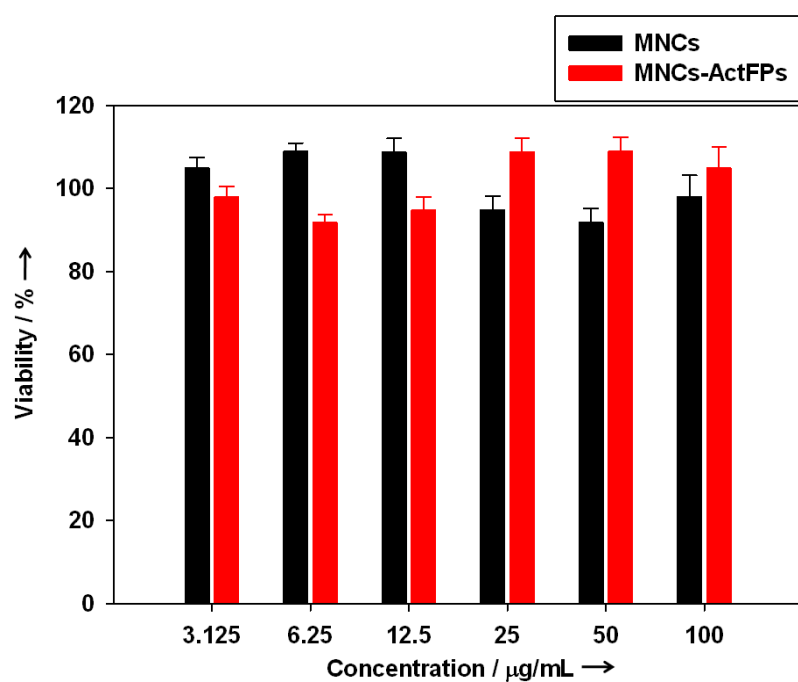


Figure S7. Cell viability by MTT assay for MNCs and MNC-ActFPs

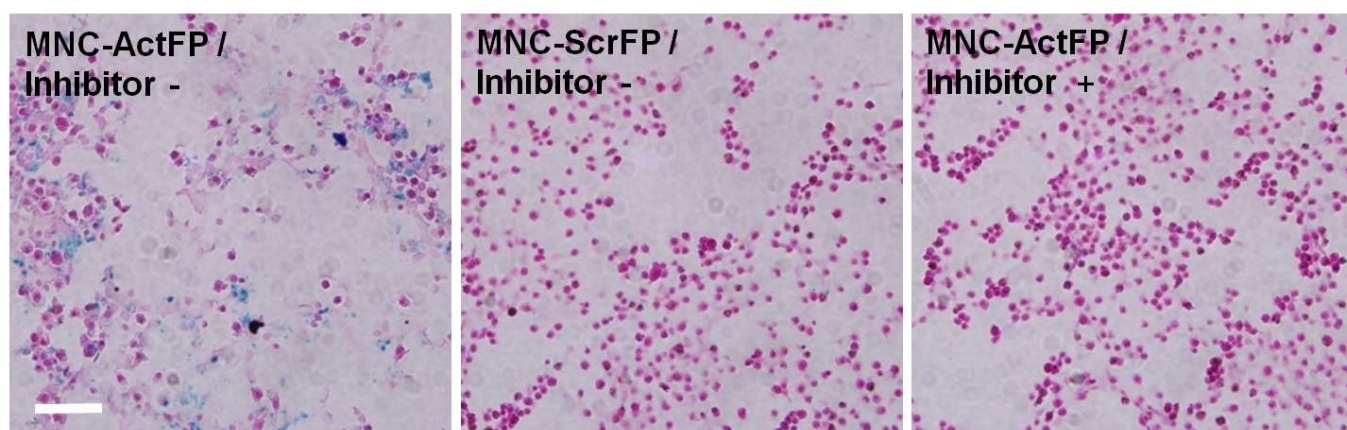


Figure S8. Prussian blue-stained image for HT1080 cells treated with MNC-ActFP, MNC-ScrFP, and MNC-ActFP with inhibitor (scale bar; 100  $\mu$ m).

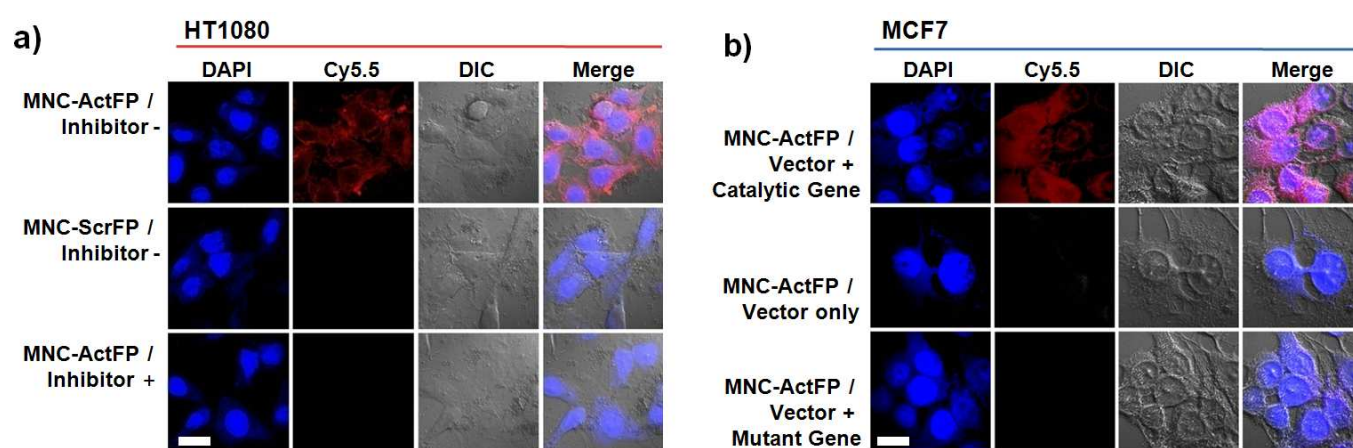


Figure S9. Confocal microscopic images for a) HT1080 and b) MCF7 cells treated with MNC-ActFP, MNC-ScrFP, and MNC-ActFP with an inhibitor, respectively (scale bar; 1  $\mu$ m). MT1-MMP (red, Cy5.5) and nucleus (blue, DAPI).

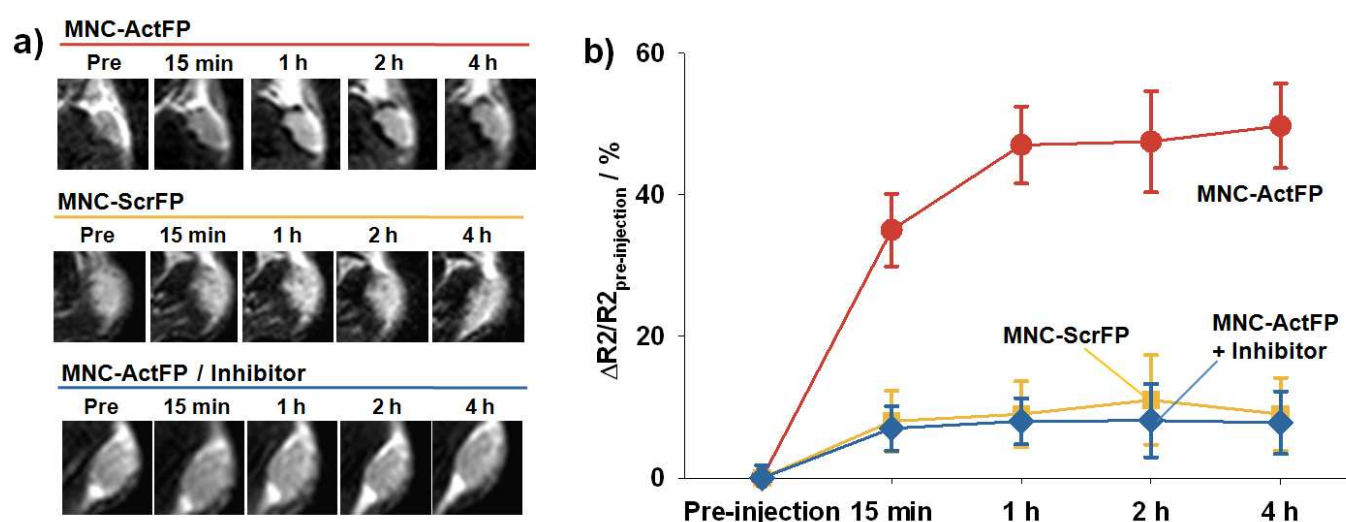


Figure S10. a) *In vivo* MR images of tumor-bearing mice after intravenous injection of MNC-ActFP, MNC-ScrFP, and MNC-ActFP + inhibitor (200  $\mu$ g Fe+ Mn per mouse), respectively, at different time points (pre-injection, 15 min, 1 h, 2 h, and 4 h) and b)  $\Delta R2/R2_{\text{non-treatment}}$  graph.

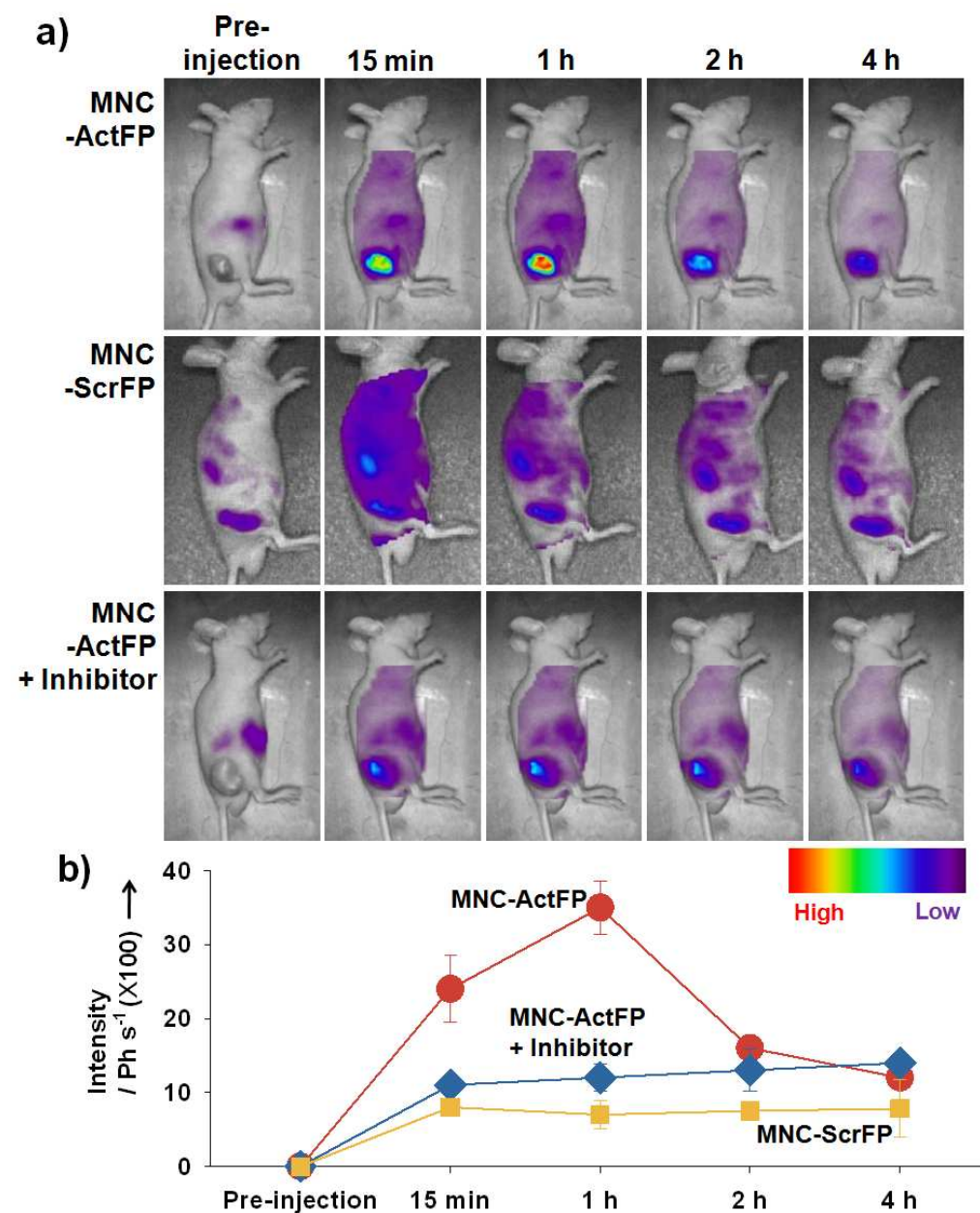


Figure S11. a) *In vivo* NIR fluorescence images of tumor-bearing mice after intravenous injection of MNC-ActFP, MNC-ScrFP and MNC-ActFP + inhibitor (200  $\mu$ g Fe+ Mn per mouse), respectively, at different time points (pre-injection, 15 min, 1 h, 2 h, and 4 h) and b) NIR fluorescence intensity graph.

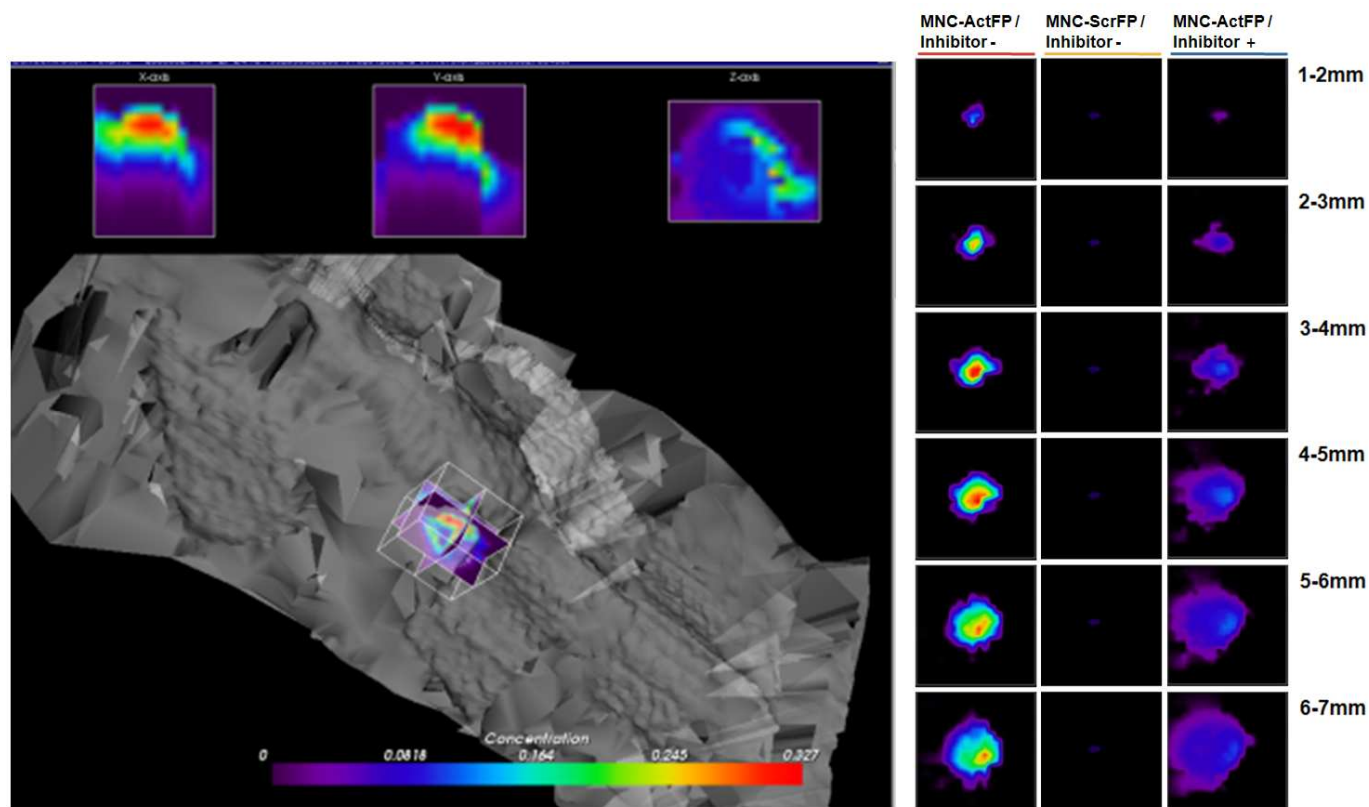


Figure S12. 3D construction images treated with MNC-ActFPs, 2-dimensional slices of the tumor images from Figure 3a reconstructed in the z direction (1-7 mm).

- [1] S. Ohkubo, K. Miyadera, Y. Sugimoto, K.-i. Matsuo, K. Wierzba, Y. Yamada, *Biochemical and Biophysical Research Communications* **1999**, 266, 308.
- [2] S. Lee, K. Park, S.-Y. Lee, J. H. Ryu, J. W. Park, H. J. Ahn, I. C. Kwon, I.-C. Youn, K. Kim, K. Choi, *Bioconjug Chem.* **2008**, 19, 1743.
- [3] R. B. Merrifield, *J. Am. Chem. Soc.* **1963**, 85, 2149.
- [4] J. Yang, C.-H. Lee, H.-J. Ko, J.-S. Suh, H.-G. Yoon, K. Lee, Y.-M. Huh, S. Haam, *Angew. Chem.-Int. Edit.* **2007**, 46, 8836.
- [5] E.-K. Lim, J. Yang, J.-S. Suh, Y.-M. Huh, S. Haam, *J Mater Chem.* **2009**, 19, 8958.